

Modelling fruit surface temperature by means of LiDAR 4D point clouds

¹N. Tapia-Zapata, ¹M. Zude-Sasse

¹Leibniz Institute for Agricultural Engineering and Bioeconomy (ATB), Department of Agromechatronics, Germany

Abstract

During the last years, the occurrence of marked heat waves has increased as a consequence of climate change. Such temperature hot spots can lead to sunburn at fruit surface. By using remote sensing techniques, real-time fruit monitoring in orchards has proven to be a data source in adapting measures against triggers of heat damage, thus creating opportunities for risk models in orchard management. Thereof, light detection and ranging (LiDAR) scanning provides geometric and radiometric information at fruit level by means of 3D point clouds. By merging LiDAR scanning and thermal imaging, 4D point clouds including temperature annotation can describe the spatial temperature distribution. Local temperature at the surface of the scanned apples was assessed by using a geometric modelling approach based on Fourier series expansion, thus expressing the apple geometry as a 2D surface in spherical coordinates. The applicability of fruit data for constructing a heat transfer model to predict fruit surface temperature is discussed using LiDAR derived fruit information at given climate conditions and growing stage. Influences due to direct and diffuse radiation at the fruit surface were observed as an increase in fruit surface temperature at specific locations in the orchard.

Keywords: LiDAR; 4D point clouds; heat transfer; radiation; convection; conduction.

INTRODUCTION

As a consequence of climate change, marked heat waves have been registered across the globe during fruit growing seasons, increasing the risk of food loss due to abiotic stresses and related damages such as sunburn. Elevated temperature can accelerate ripening process, leading to premature fruit drop, and reducing quality of produce (Morales-Quintana et al., 2020). The integration of remote sensing technologies and advanced modelling techniques offer a synergistic approach to enhance fruit management, providing real-time data on orchards. Such integrated approach enables predictive insights for more informed decision-making in response to marked heat waves during summer season.

Recent advances in terrestrial remote sensing in precision horticulture has been used in fruit identification and counting by using image processing and laser scanning (Miranda et al., 2023). Additionally, thermal imaging can aid real time temperature and wetness at fruit level to identify potential hot spots during the growing season (Stajniko et al., 2004; Ranjan et al., 2022). Further advances in light detection and ranging (LiDAR) provide 3D point clouds in space of entire canopy regions. Furthermore, individual tree part segmentation into wood, leaves and fruit have been performed using geometric and radiometric characteristics of point clouds (Tsoulias et al., 2020). Most important, multi-sensor merging has been developed by fusing LiDAR scanning and thermal imaging, obtaining temperature annotation in each point within a point cloud after intrinsic and extrinsic calibration between LiDAR and thermal imaging (Tsoulias et al., 2022). Thus, 4D point clouds can provide temperature at the surface of segmented fruit as a multi-dimensional point cloud. Additionally, geometric models to approximate fruit centroid by

means of 3D point clouds has been developed to predict apple size using Fourier series expansion (Tapia-Zapata et al., 2022). Altogether, time series of temperature at fruit surface during fruit growth development can serve as a new tool to develop risk-models at fruit level by means of 4D point clouds.

The prediction modelling of temperature at fruit surface in extreme weather conditions remains a considerable challenge due to multiple factors affecting heat transfer at surface level. Moreover, the relative contribution of environmental and weather conditions on the rate of heat transfer by various mechanisms remain a complex task. Additionally, intrinsic thermal and optical characteristic of the produce can also affect heat transfer rate. Typically, heat transfer in fruits can be expressed considering Newton's law of energy conservation. Thereof, radiative, convective and conductive heat transfer mechanisms play a significant role (Smart and Sinclair, 1976).

The objective of this research was the description of temperature at apple surface by means of Fourier analysis of LiDAR 4D point clouds at different growth stages and location in the orchard during fruit development on the tree. Additionally, a modelling approach to predict temperature at apple surface is proposed.

MATERIALS AND METHODS

Data acquisition

Thermal imaging and LiDAR scanning were conducted at the Leibniz Institute for Agricultural Engineering and Bioeconomy (ATB), Field Lab for Digital Agriculture, located in Potsdam-Marquardt, Germany (52.466329 N, 12.959194 E, 39 m altitude). Data were taken from an open access data base (Zude-Sasse et al., 2024). For this experiment, two blocks of three consecutive apple trees of 'Gala' located at opposite extremes of the tree row were considered at both left and right sides of the tree row, in order to capture spatial variability within the tree row (Figure 1). All trees were trained as slender spindle with average distance between trees and height of 0.95 and 2.5 m, respectively. The tree rows in the orchard are oriented in the NO-SE direction and distance between rows of 5 m.

The 3D point cloud of all monitored blocks were obtained by means of a mobile 2D LiDAR system (LMS-511, Sick AG, Waldkirch, Germany) emitting at wavelength of 905 nm with angular resolution of 0.1667° and 25 Hz scanning frequency. Thermal imaging was performed using a thermal camera (A655sc, FLIR Systems Inc., MA, USA) with a spatial resolution of 640 x 480 pixels, operational temperature ranging from -40 to 150 °C and thermal resolution < 0.05 °C. Additionally, a lens (T198065, FLIR Systems INC., MA, USA) with a focal length of 6.5 mm (diagonal 80°) was attached to the thermal camera. The LiDAR system and the thermal camera were mounted on a circular conveyor system using an electrical engine at 50 Hz frequency (DRN71, SEW Eurodrive, Germany). The conveyor moved at constant speed of 10 mm/s and apparent distance between the sensors and the trees of 2.0 m. The blocks were monitored at 67, 81, 117, 132 and 136 days after full bloom (DAFB) during fruit development (date of full bloom: 23rd of April, 2022).

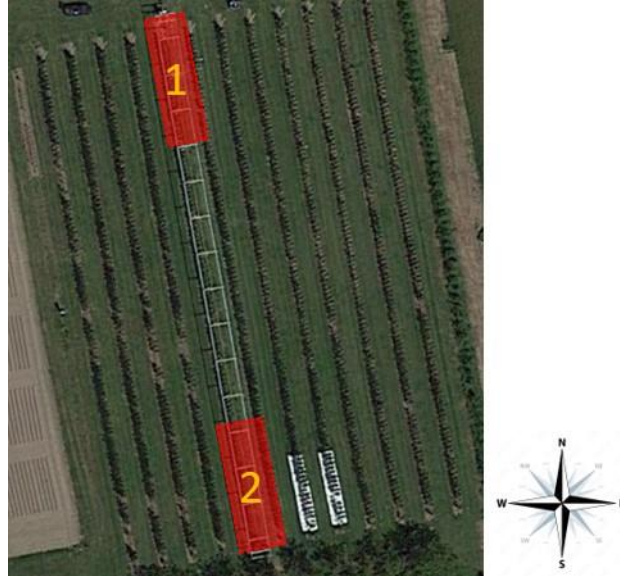


Figure 1. Satellite image of the experimental plot (Google, n.d.). Monitored block of trees are denoted in red.

Temperature annotation into all point clouds was performed by intrinsic and extrinsic calibration of the thermal camera and the LiDAR scanner (Tsoulias et al., 2022). Subsequently, all point clouds that belonged to an apple were segmented based on their radiometric and geometric properties (Tsoulias et al., 2020).

Date and measuring hour were registered for all the studied growth stages (Table 1). Additionally, air temperature T_{air} ($^{\circ}\text{C}$), global radiation R_G (W/m^2), and wind speed u (m/s) and direction were recorded hourly by a weather station in the experimental field (UNIKLIMA vario, TOSS Ltd., Potsdam, Germany), for all studied growth stages.

Data postprocessing

Using 294 T-annotated point clouds of apples, a Fourier based approach was used to approximate the apparent apple centroid (Tapia-Zapata et al., 2022). After approximation, all point clouds of the form $P(x, y, z)$ were expressed in spherical coordinates of the form $R(\theta, \phi)$ and $T(\theta, \phi)$ for apple radius and temperature, respectively. Angles of θ and ϕ represent azimuth and elevation, respectively. The elevation angle ϕ starts from the stem of the apple to its calix, from $\phi = 0$ to $\phi = \pi$. Likewise, the angle of azimuth θ has a period of 2π , starting and ending at the back of the point cloud, thus locating the measured face of the apple in the middle of aspherical plane – where $\theta = \pi$.

Table 1. Date, time of scanning and total number of segmented apples for all blocks at all studied growing stages.

	Date	Measurement time				Total segmented apples
		Block 1		Block 2		
		Left	Right	Left	Right	
<i>DAFB</i> ₆₇	28.06	09:20 – 09:28	09:51 – 09:55	10:02 – 10:07	10:35 – 10:40	56
<i>DAFB</i> ₈₁	12.07	07:55 – 08:03	08:37 – 08:42	08:45 – 08:49	08:30 – 08:35	59
<i>DAFB</i> ₁₁₇	17.08	11:31 – 11:37	12:12 – 12:17	11:32 – 11:37	12:00 – 12:06	63
<i>DAFB</i> ₁₃₂	01.09	07:20 – 07:24	09:31 – 09:34	07:27 – 07:31	09:24 – 09:27	58
<i>DAFB</i> ₁₃₆	06.09	07:39 – 07:45	09:50 – 09:55	07:51 – 07:55	09:39 – 09:45	58

Model description

A steady-state energy balance model was proposed to predict apple surface temperature. In this context, the model considered the heat intake due to radiation ($E_{radiation}$), and heat losses due to convection ($E_{convection}$) and emitted short-wave radiation ($E_{emittedrad}$). At the present stage, heat loss due to transpiration and conduction were not included, as the energy balance is performed a single moment in time (Li et al., 2014). The energy balance according to Newton's law of energy conservation is described as:

$$E_{radiation} = E_{emittedrad} + E_{convection} \quad (1)$$

Where the outgoing short-wave radiation from the apple surface is estimated as:

$$E_{emittedrad} = \varepsilon_{fs} \cdot \sigma \cdot (T_{fs} + 273)^4 \quad (2)$$

Where ε_{fs} is the emissivity of the fruit, σ is the Stefan-Boltzmann constant ($5.67 \cdot 10^{-8} \text{ W/m}^2 \text{ }^\circ\text{C}^4$) and T is the temperature at fruit surface ($^\circ\text{C}$). Energy loss due to convection from the apple surface was determined by:

$$E_{convection} = c_p \cdot g_a \cdot (T_{fs} - T_{air}) \quad (3)$$

Where c_p is the heat capacity of the ambient air ($\text{J/mol}\cdot^\circ\text{C}$), g_a is the turbulence conductance of the air at the boundary layer (-), T_{air} and T_{fs} represent the temperature of the air and at the fruit surface, respectively. Typically for spherical objects, g_a is estimated as:

$$g_a = 1.4 \cdot 0.135 \cdot \sqrt{\frac{u}{d}} \quad (4)$$

Where u is the wind speed (m/s) – measured from the weather station – and d is the characteristic length of the object. For apples, values of d were defined as the predicted apple diameter derived from Fourier analysis multiplied by a correction factor of 0.84 (Evans, 2004).

Total incoming radiation at the apple surface consists of the sum of short and long wave radiation – namely R_s and R_l , respectively (W/m^2). For an apple within a canopy, the ratio of radiation intake by the apple is given by the proportion of the apple area exposed

to both radiation from direct sunlight and reflected radiation from the canopy and the ground. The short-wave radiation intake is given by:

$$R_s = \frac{A_{sunlit}}{A_{LiDAR}} (1 - \alpha) R_G \quad (5)$$

Where A_{sunlit} is the projected area of the apple that receives direct sunlight, A_{LiDAR} is the area of the apple scanned by the LiDAR, which is assumed to be the maximum exposed area of the apple in the direction of the incident sunlight. The reflectance of the apple surface α was set to be 0.6 (Evans, 2004) and R_G is the direct short wave radiation, calculated by dividing the global radiation (W/m^2) by the sine of the elevation angle (β) of the sun at a given day during the year. The energy intake due to long wave radiation by the apple surface was defined as:

$$R_l = \varepsilon_a \cdot \sigma \cdot (T_{air} + 273)^4 + \frac{A_{shaded}}{A_{apple}} \varepsilon_g \cdot \sigma \cdot (T_{air} + 273)^4 \quad (6)$$

Where A_{shaded} is the area of the apple exposed to reflected radiation from the ground and canopy, and A_{apple} is the total surface area of the apple. Variables ε_a and ε_g represent the emissivity of the atmosphere and ground, respectively.

Boundary conditions model and solving algorithm

The effect of direct sunlight was determined according to the time of scanning during the day. Additionally, values of emissivity and albedo of the apple were kept constant for all simulated scenarios. Effect of airflow resistances on effective air velocity in the canopy were not considered for these simulations. Scanned areas of the apples by means of approximated point clouds was performed using an alphashape algorithm in conjunction with Haversine formula for the estimation of spherical regions (Edelsbrunner et al., 1983; Miller, 1994).

The resulting energy balance to solve for the mean fruit surface temperature T_{fs} was performed by re-arranging eq. 1 by means of eqs. 2-6: The resulting quadratic equation was iteratively solved using the Newton Raphson method as:

$$T_{fs} = \frac{E_{radiation} - \varepsilon_{fs} \cdot \sigma \cdot (T_{fs} + 273)^4}{c_p g_a} + T_{air} \quad (7)$$

An error tolerance of $1E-8$ was established between iterations when finding the root of equation 7. The model was tested using averaged size and exposed area (A_{LiDAR}).

RESULTS AND DISCUSSION

Average size and local temperature at the apple surface were determined for each apple point cloud in various growth stages using spherical coordinates (Figure 2). During the measuring period, the size of apples increased. Apple mean approximated radius and temperature were obtained for all studied growing stages (Table 2). Estimated apple size was set as input for the heat transfer model, for each growing stage.

Representing the apple geometry as an ideal sphere of known radius can serve as a boundary condition for heat transfer due to conduction at a given day. Additionally, the projection of each point cloud in the spherical plane indicated how much of the apple is potentially exposed to direct radiation. The scanned surface indicates the region of the apple exposed

to direct forced convection due to airflow. However, more detailed information regarding local velocity must be accounted for at different locations within an orchard.

Table 2. LiDAR derived mean apple size and temperature at all studied growing stages.

	<i>DAFB</i> ₆₇	<i>DAFB</i> ₈₁	<i>DAFB</i> ₁₁₇	<i>DAFB</i> ₁₃₂	<i>DAFB</i> ₁₃₆
Mean approximated radius (mm)	25.8 ± 10.5	27.4 ± 8.1	30.9 ± 8.2	35.3 ± 9.6	35.5 ± 7.3
Mean surface temperature (°C)	29.1 ± 7.7	28.8 ± 4.2	29.2 ± 1.9	23.5 ± 3.3	14.6 ± 1.7

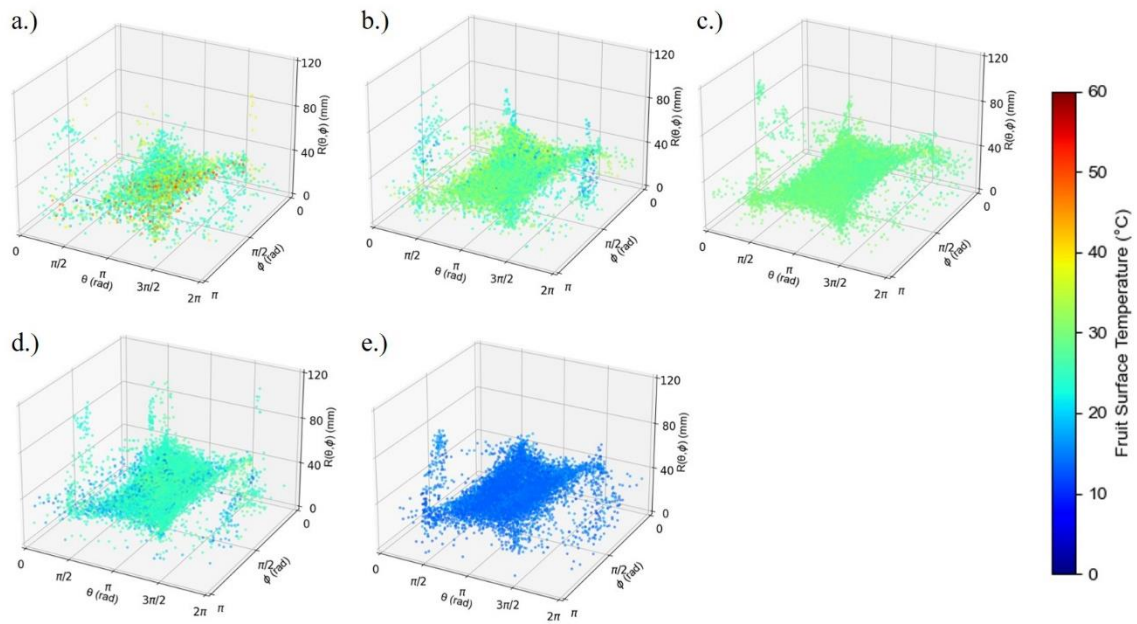


Figure 2. Apple point clouds in spherical coordinates after centroid approximation for: a.) *DAFB*₆₇, b.) *DAFB*₈₁, c.) *DAFB*₁₁₇, d.) *DAFB*₁₃₂ and e.) *DAFB*₁₃₆.

The model successfully simulated the fruit surface temperature at all monitored growing stages. At 67 DAFB, differences in mean temperatures up to 22 % were observed between right and left side of the row, obtained from scanned apples around 10:30 AM (Figure 3a). Moreover, local differences on apple surface temperature up to 38 % were observed between apples on the left and right side of the canopy. At this growing stage, a large increase in the apple size was observed, increasing the radiation intake at apple surface due to direct radiation. Thereof, the exposed area of the apple to direct solar radiation must be accounted for locally, estimating the time of the day and duration of direct sunlight exposure at fruit surface. On the contrary, the model overpredicted the apple surface temperature by approximately 34 % at 136 DAFB (Figure 3e). At low registered global radiation, the effective area of the apple exposed to direct radiation was overestimated, affecting the predicted surface temperature of the apple. Moreover, the radiation heat absorbed by the fruit surface was found to be significant. The rate of heat transfer due to

direct radiation depends not only on the global radiation level, but also on the region of the exposed fruit that receives direct sun radiation at a given solar time.

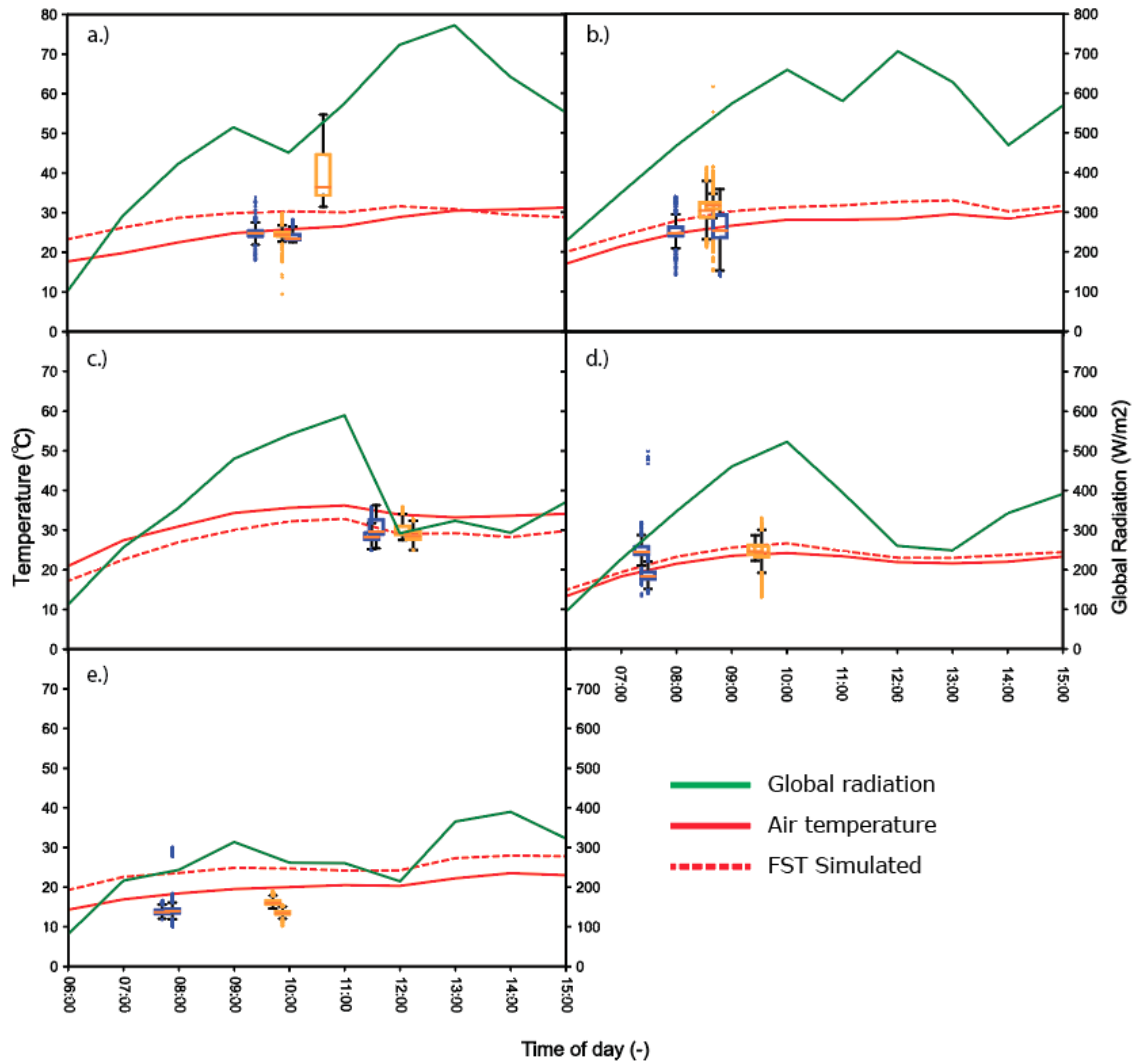


Figure 3. Annotated apple fruit surface point cloud temperature (FST) for blocks 1 (blue) and 2 (orange). Additional hourly measurements of air temperature (°C) (red line) and global radiation (W/m²) (green line) were registered for a.) *DAFB*₆₇, b.) *DAFB*₈₁, c.) *DAFB*₁₁₇, d.) *DAFB*₁₃₂ and e.) *DAFB*₁₃₆.

In addition to the effects of radiation on the model performance, the model accounted for the effect of convection on the apple surface temperature. Up to 3 % differences between predicted and LiDAR scanned temperature were observed at 117 *DAFB* (Figure 3c). At this stage, wind speeds of 0.8 m/s were registered. However, the airflow direction was majorly encountered to be parallel to the row of trees, thus enhancing convective cooling (Figure 4a). On the contrary, high wind speeds of 1.7 and 1.4 m/s were observed at *DAFB*₆₇ and *DAFB*₈₁, respectively. However, the direction of the wind at these days was towards west, almost perpendicular to the row of trees. Thus, wind direction was found as relevant as wind speed when considering heat transfer. Moreover, the effective superficial velocity at the fruit surface could be estimated to some degree of accuracy by more detailed modelling approaches, such as Computer Fluid Dynamics (CFD) (Atam et al., 2020; Xu et

al., 2022). Using the spatially resolved temperature distribution in orchards may provide a new data source for thermodynamic models, accounting for local changes in direct short-wave radiation and effective airflow velocity.

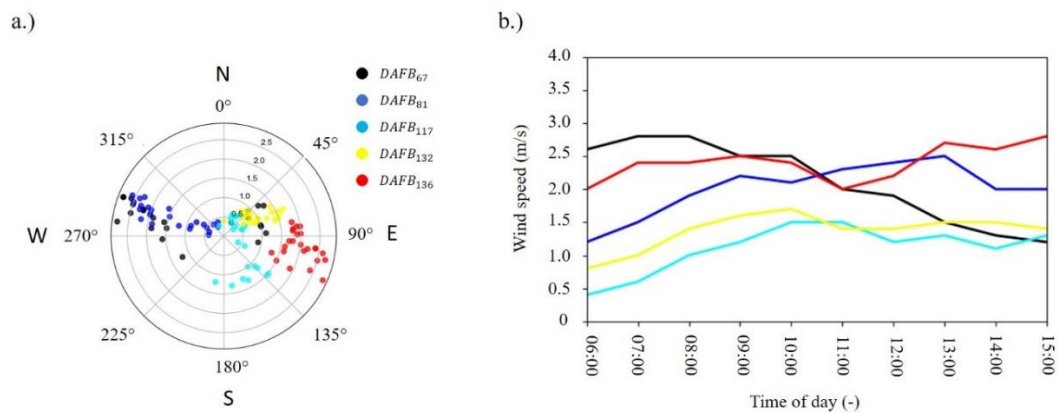


Figure 4. a.) Registered wind speed and direction for all studied growing stages, and b.) hourly registered wind speed at the orchard.

CONCLUSIONS

A thermodynamic modelling scheme was presented to predict apple surface temperature by means of LiDAR 4D point clouds. The model considered radiative and convective heat transfer using weather data and fruit size as input. Overall good agreement was found between predicted and measured fruit temperature using the 4D point clouds. Moreover, direct radiation at fruit surface was found to be relevant when simulating apple surface temperature. Differences up to 22 % were found between predicted and simulated fruit surface temperature at 67 DAFB, where direct beam radiation had an effect on apple surface temperature for highly exposed fruit. In addition to radiation, the model accounted for the effect of convection on heat transfer at 117 DAFB, where the wind speed was found to be majorly oriented in the direction of the tree rows. Differences between predicted and LiDAR apple surface temperature of 3 % were observed. Further work on data collection at different times is required. More specifically, the model shall be validated for each scanned apple at multiple solar hours (sunrise, solar noon, sunset), for each considered DAFB. Moreover, further modelling work on local airflow around apples within orchards are required for an accurate temperature prediction.

Bibliography

- Atam, Ercan, Se-Woon Hong, and Alessia Arteconi. 2020. 'Thermofluid Modelling of Large-Scale Orchards for Optimal Design and Control of Active Frost Prevention Systems', *Energies*, 13: 378.
- Caliskan-Aydogan, Ozgur, Hojae Yi, James R. Schupp, Daeun Choi, Paul H. Heinemann, and Virendra M. Puri. 2020. 'Thermal Properties of 'Gala' Apples during Growing Season for Predicting Harvest Time', *Transactions of the ASABE*, 63: 305-15.
- Edelsbrunner, H., D. Kirkpatrick, and R. Seidel. 1983. 'On the shape of a set of points in the plane', *IEEE Transactions on Information Theory*, 29: 551-59.
- Evans, R. G. 2004. 'ENERGY BALANCE OF APPLES UNDER EVAPORATIVE COOLING', *Transactions of the ASAE*, 47: 1029-37.
- Google. n.d. [Field Lab for Digital Agriculture, located in Potsdam-Marquardt, Germany (52.466329 N, 12.959194 E)]. (01 December 2023). Google Maps. Google.

- Li, Lei, Troy Peters, Qin Zhang, Jingjin Zhang, and Danfeng Huang. 2014. 'Modeling apple surface temperature dynamics based on weather data', *Sensors*, 14: 20217-34.
- Lisowa, H., M. Wujec, and T. Lis. 2002. 'Influence of temperature and variety on the thermal properties of apples', *International Agrophysics*, 16: 43-52.
- Miller, Robert D. 1994. 'II.4. - Computing the Area of a Spherical Polygon.' in Paul S. Heckbert (ed.), *Graphics Gems* (Academic Press).
- Miranda, Juan C., Jordi Gené-Mola, Manuela Zude-Sasse, Nikos Tsoulias, Alexandre Escolà, Jaume Arnó, Joan R. Rosell-Polo, Ricardo Sanz-Cortiella, José A. Martínez-Casasnovas, and Eduard Gregorio. 2023. 'Fruit sizing using AI: A review of methods and challenges', *Postharvest Biology and Technology*, 206: 112587.
- Morales-Quintana, Luis, Jessica M. Waite, Lee Kalcsits, Carolina A. Torres, and Patricio Ramos. 2020. 'Sun injury on apple fruit: Physiological, biochemical and molecular advances, and future challenges', *Scientia Horticulturae*, 260: 108866.
- Nobel, P. S. 1975. 'Effective thickness and resistance of the air boundary layer adjacent to spherical plant parts', *Journal of Experimental Botany*, 26: 120-30.
- Ranjan, Rakesh, Rajeev Sinha, Lav R. Khot, and Matthew Whiting. 2022. 'Thermal-RGB imagery and in-field weather sensing derived sweet cherry wetness prediction model', *Scientia Horticulturae*, 294: 110782.
- Smart, Richard E., and Thomas R. Sinclair. 1976. 'Solar heating of grape berries and other spherical fruits', *Agricultural Meteorology*, 17: 241-59.
- Stajnko, D., M. Lakota, and M. Hočevár. 2004. 'Estimation of number and diameter of apple fruits in an orchard during the growing season by thermal imaging', *Computers and Electronics in Agriculture*, 42: 31-42.
- Tsoulias, Nikos, Sven Jörissen, and Andreas Nüchter. 2022. 'An approach for monitoring temperature on fruit surface by means of thermal point cloud', *MethodsX*, 9: 101712.
- Tsoulias, Nikos, Dimitrios S. Paraforos, George Xanthopoulos, and Manuela Zude-Sasse. 2020. 'Apple shape detection based on geometric and radiometric features using a LiDAR laser scanner', *Remote Sensing*, 12: 2481.
- Xu, Tao, Hao Zhou, Xiaolan Lv, Xiaohui Lei, and Shutian Tao. 2022. 'Study of the Distribution Characteristics of the Airflow Field in Tree Canopies Based on the CFD Model', *Agronomy*, 12: 3072.
- Zapata, N. T., N. Tsoulias, K. K. Saha, and M. Zude-Sasse. 2022. "Fourier analysis of LiDAR scanned 3D point cloud data for surface reconstruction and fruit size estimation." In *2022 IEEE Workshop on Metrology for Agriculture and Forestry (MetroAgriFor)*, 197-202.
- Zude-Sasse., M, Regen, C., Baranyai, L., Tsoulias, N. (2024). Temperature annotated 3D point clouds of fruit trees and segmented fruit surface temperature distributions. Data in Brief, in press